UMONS
Université de Mons

Adiponectin pathway in murine models of skeletal muscle deconditioning and reconditioning

Sébastien Szczepanski

Supervisor : Prof A Tassin

Co-supervisor : Prof A-E Declèves

Faculté de Médecine et de Pharmacie

PhRR2

BMM Lab

fnrs LA LIBERTÉ DE CHERCHER

FRMH

santé INSTITUT DE RECHERCHE EN SCIENCES ET TECHNOLOGIES DE LA SANTE DE L'UMONS

ABMM Téléthon.be

(Bodine et al., Int J Biochem Cell Biol, 2013)

ICU aquired muscle weakness (**ICUAW**)

- **Persistant muscle weakness**
- **Reduced endurance capacities**

- **Several factors implicated (mechanical ventilation, curarisation, systemic inflammation, bed rest …)**

➢ **Patient condition before ICU is critical for physical recovery**

Niké Boelens *et al. Curr Opin Crit Care* (2022)

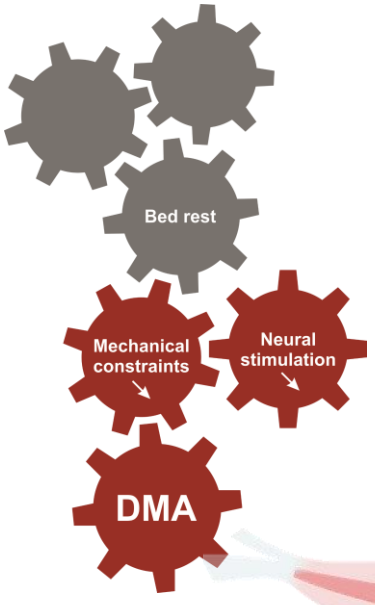

Disuse
Muscle
Atrophy

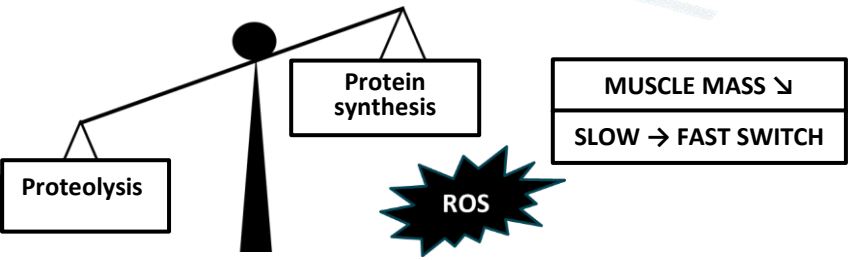

Bodine *et al*. (2013) ; Baehr *et al. Cell* (2022)

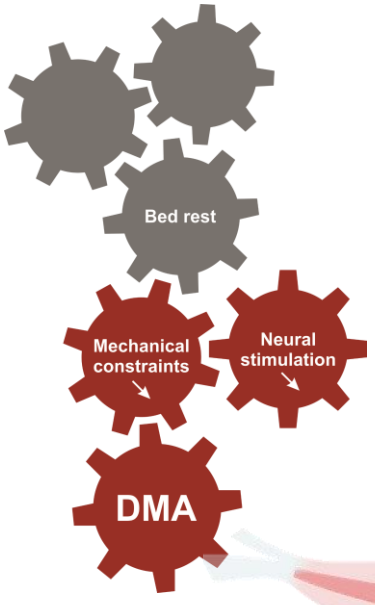

Disuse
Muscle
Atrophy

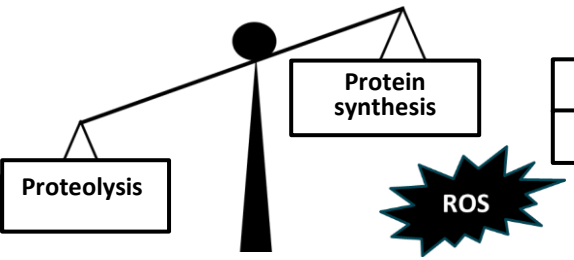

MUSCLE MASS ↘
SLOW → FAST SWITCH

Therapeutic target ?

(Nuoc et al, J Physiol Sci, 2017 ; Bodine et al., Int J Biochem Cell Biol, 2013)

ApN pathway

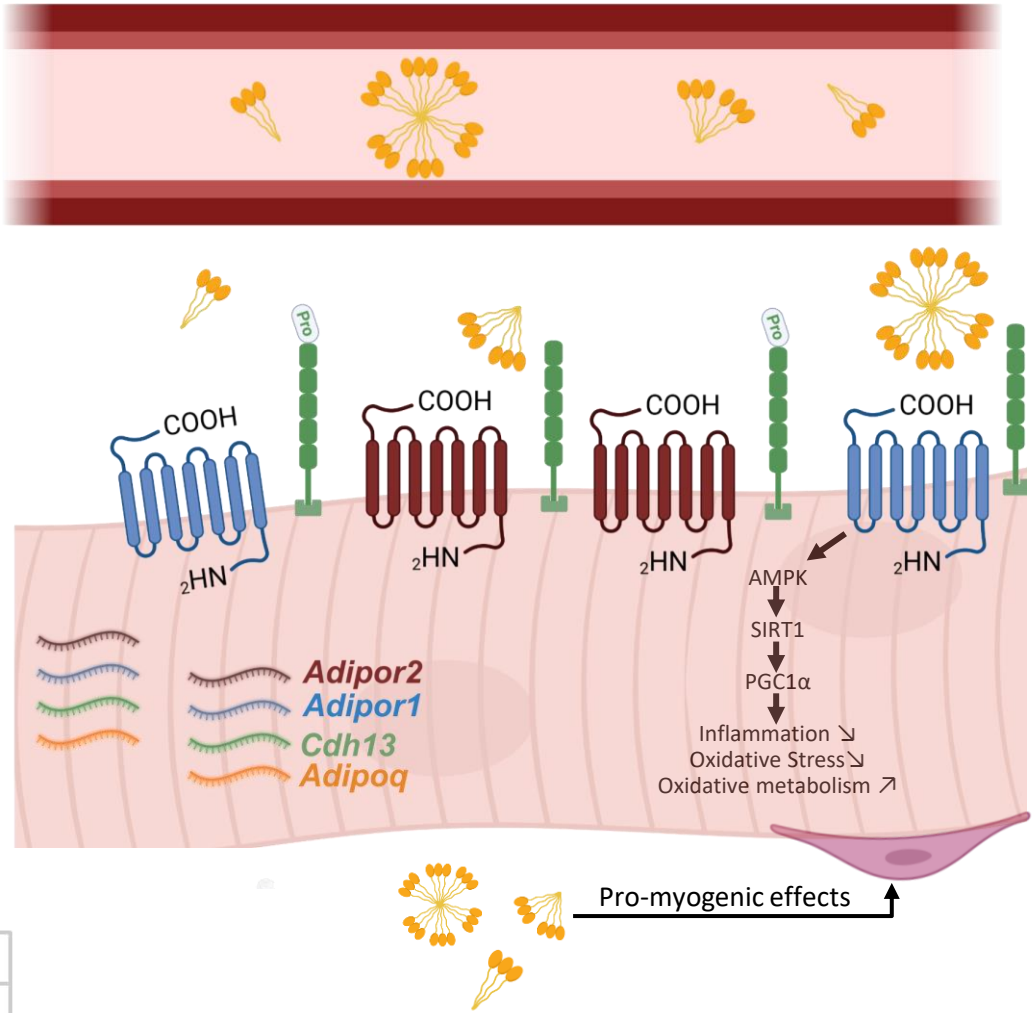

Abou-Samra *et al. Int. J. Mol. Sci.* (2020)

ApN pathway

myoprotective effects

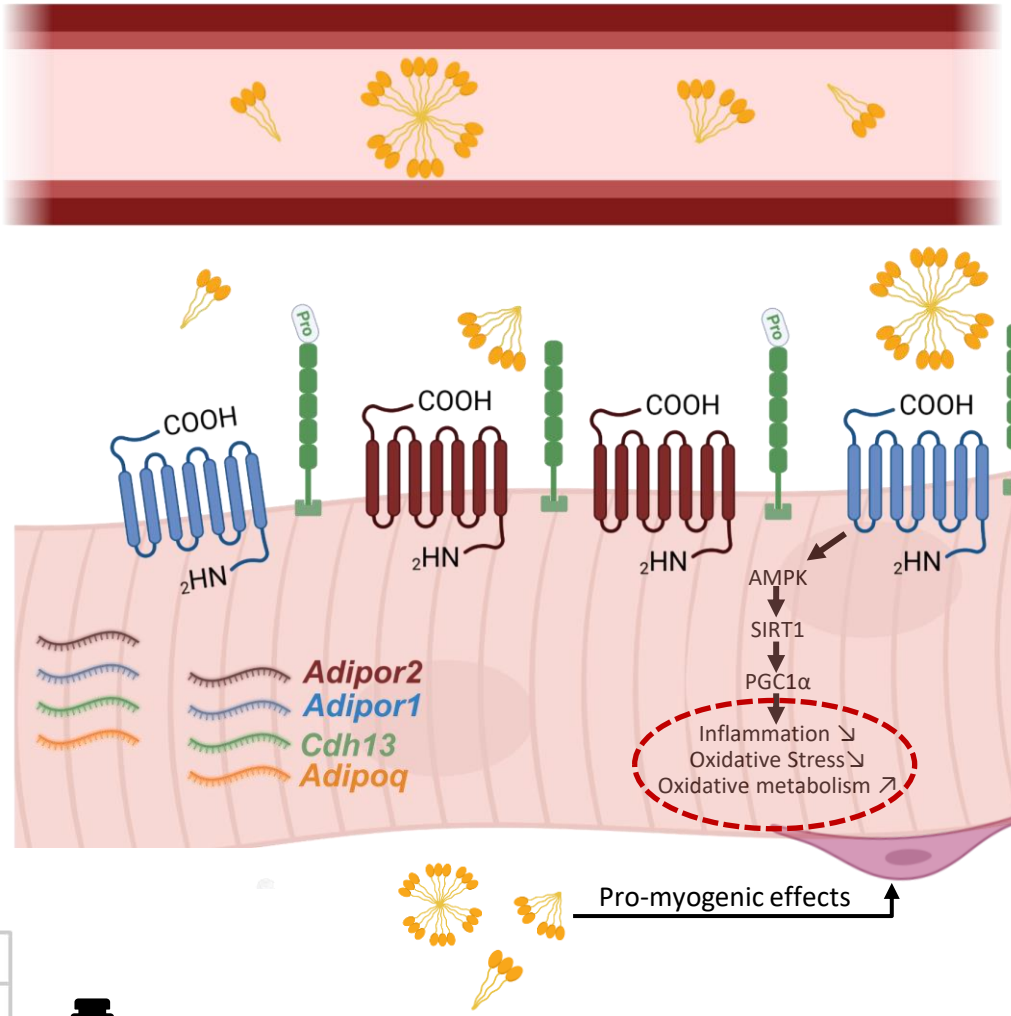

ApN agonists in *mdx* and aged mice

Abou-Samra *et al. Int. J. Mol. Sci.* (2020)

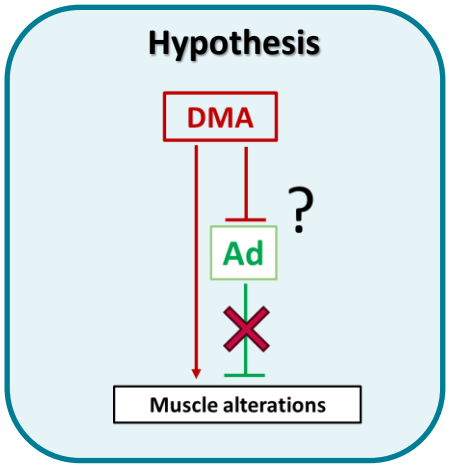

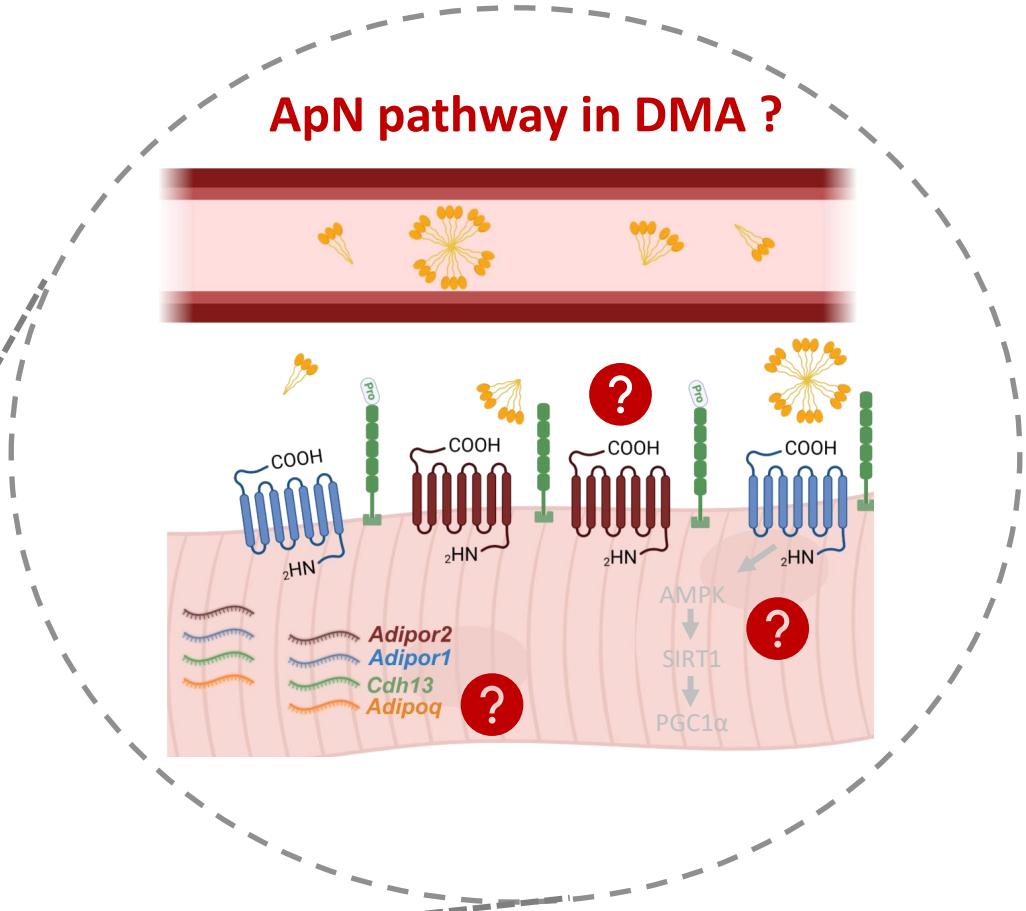

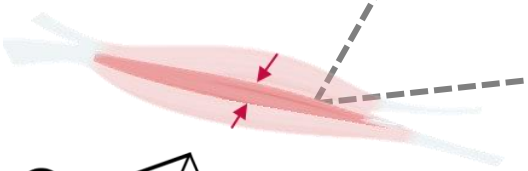

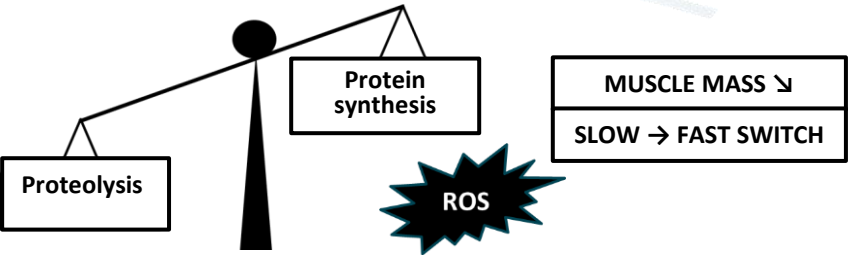

Abou-Samra *et al. Int. J. Mol. Sci.* (2020)

HindLimb Unloading and Immobilization as a DMA murine model

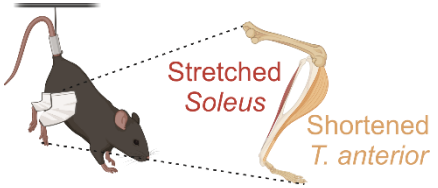

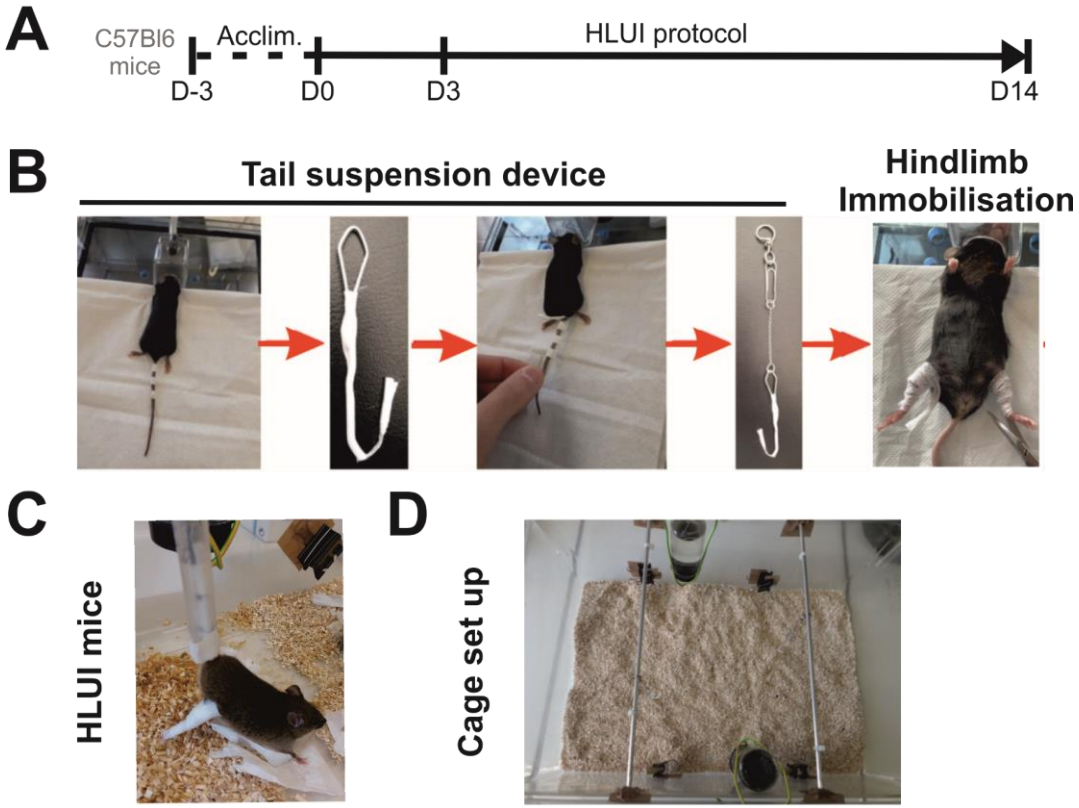

Szczepanski et al., (2024) in preparation

HLUI effect on body weight (b.w) evolution

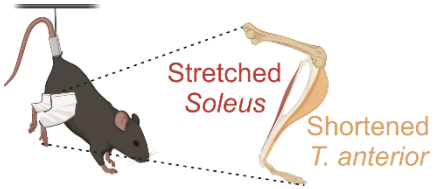

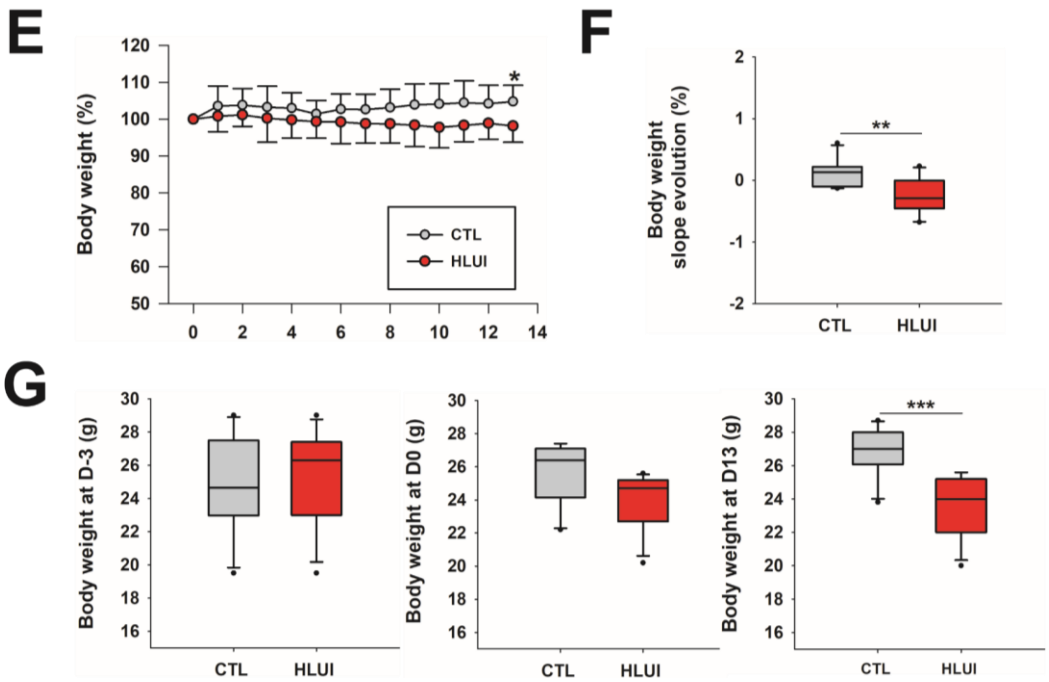

B.W at D13:
CTL (104.77 ± 4.43 %)
HLUI (98.15 ± 4.44 %)

Limited b.w decrease in HLUI mice

(E) Data represented as mean ± SEM, *: p<0.05, *CTL(n=10) vs HLUI(n=11)*, Two-way ANOVA repeated measures (D13). **(F)** Data represented as boxplots; **: p=0.005, *CTL(n=10) vs HLUI(n=11),* student's t-test. **(G)** Data represented as boxplots; ***: p<0.001, *CTL(n=10) vs HLUI(n=11),* Mann-Whitney Rank Sum test.

Szczepanski et al., (2024) in preparation

HLUI-mediated muscle disuse effects in mice *Soleus* are fibre-type dependant.

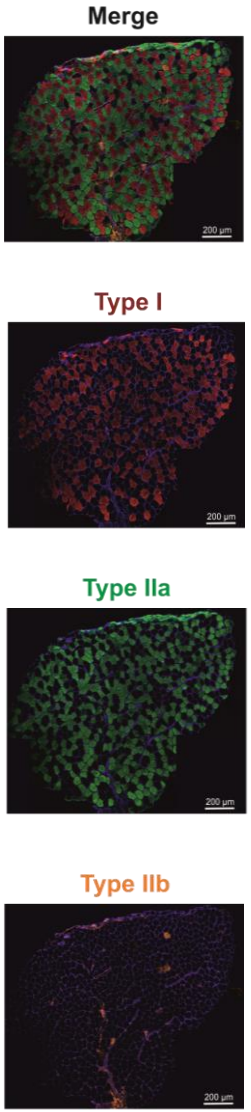

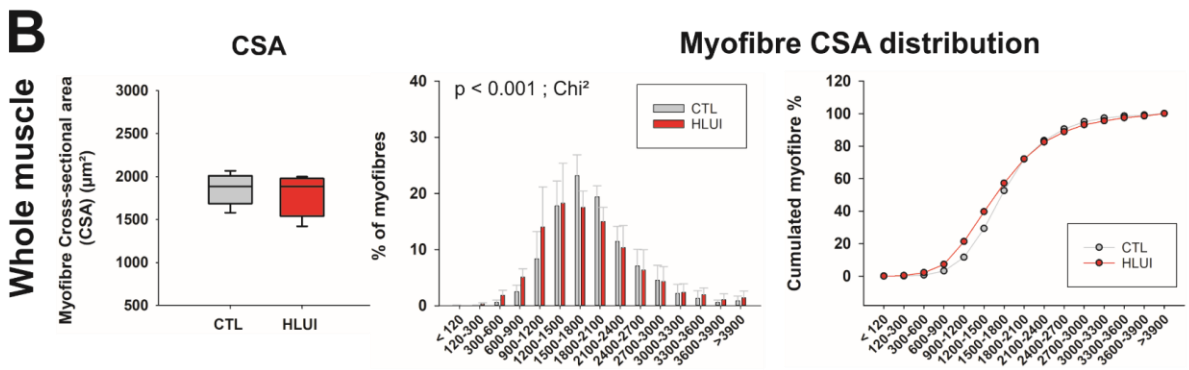

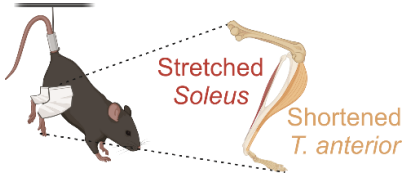

(Left) Data represented as boxplot. *CTL(n=5) vs HLUI(n=5)*, t-test, NS.
(Center) Data represented as mean ± SD, *CTL(n=5) vs HLUI(n=5)*, Chi-square.
(Right) Cumulative percentages of myofibres in clusters.

Szczepanski et al., (2024) in preparation

HLUI-mediated muscle disuse effects in mice *Soleus* are fibre-type dependant.

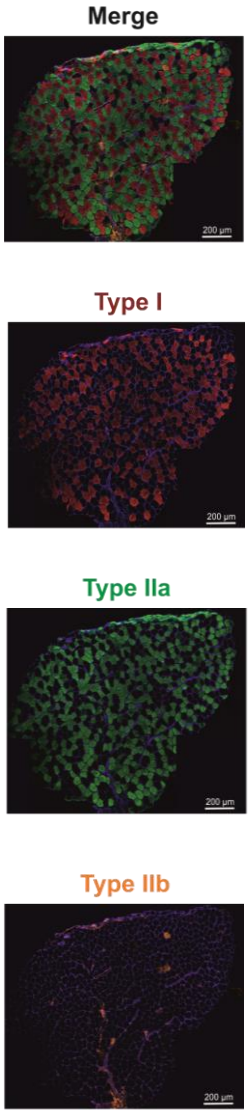

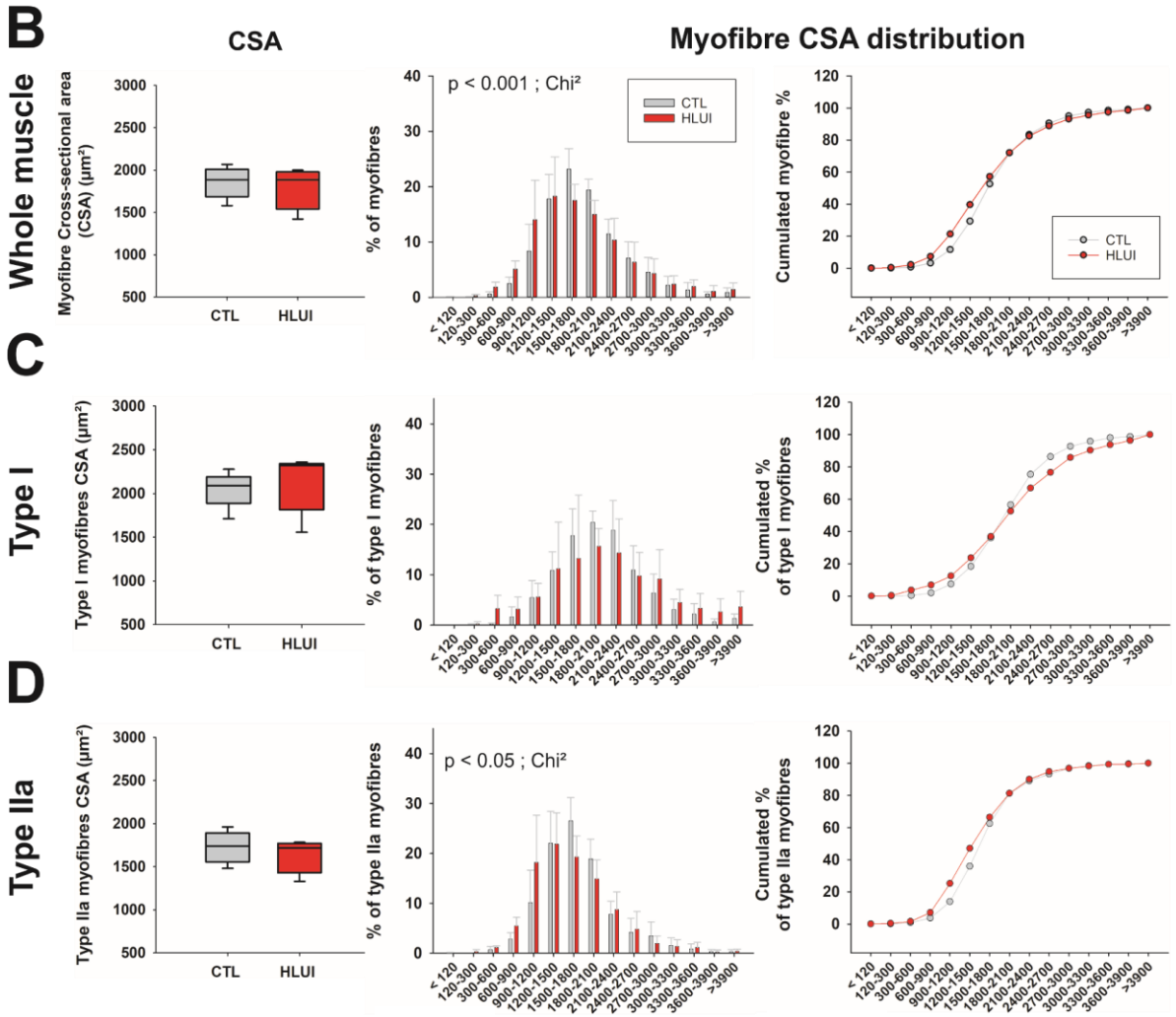

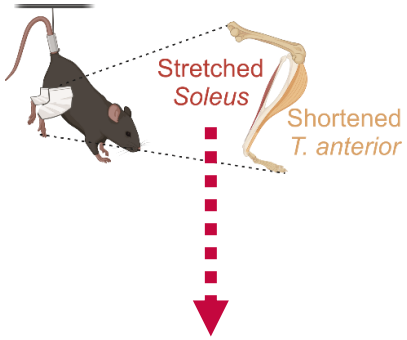

Moderated atrophy

(Left) Data represented as boxplot. *CTL(n=5) vs HLUI(n=5)*, t-test, NS.
(Center) Data represented as mean ± SD, *CTL(n=5) vs HLUI(n=5)*, Chi-square.
(Right) Cumulative percentages of myofibres in clusters.

Szczepanski et al., (2024) in preparation

HLUI-mediated muscle disuse effects in mice *Soleus* are fibre-type dependant.

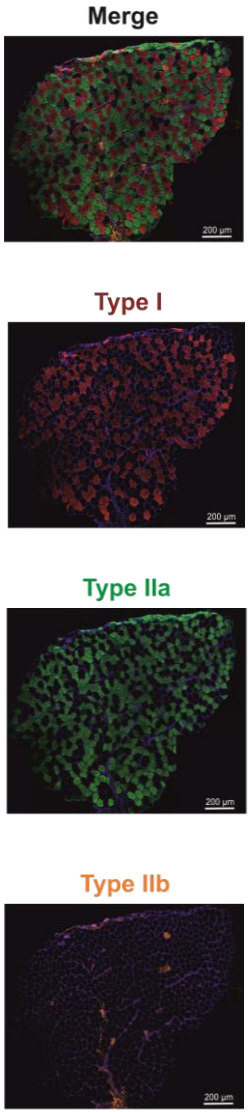

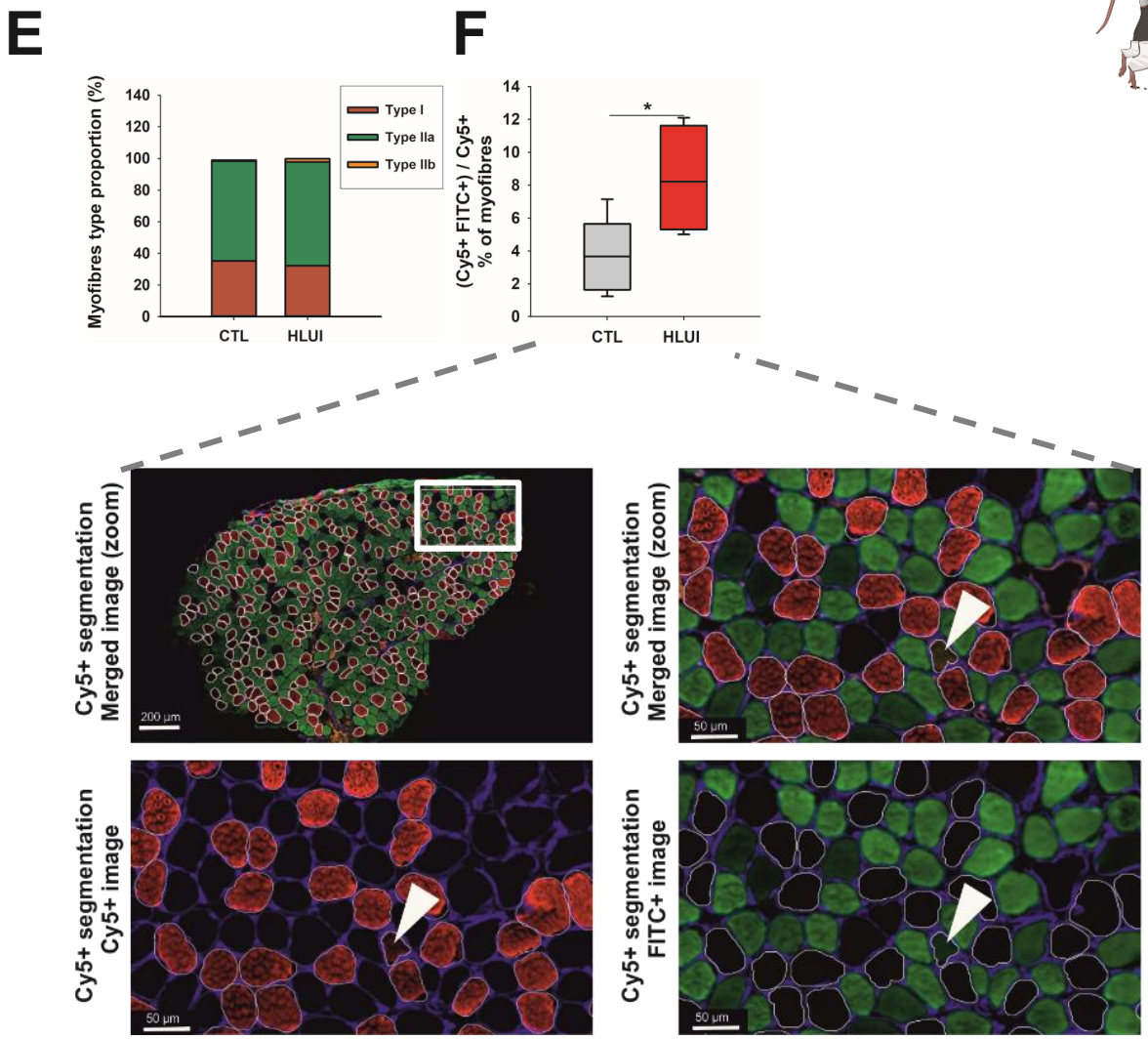

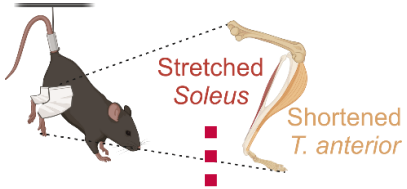

Moderated Atrophy + Ongoing Fiber-type Switch

(E) Data represented as stacked bars; *CTL(n=5) vs HLUI(n=5)* in type I, Iia and IIb myofibers, t-test, NS.
(F) Data represented as boxplot, *: p<0.05, *CTL(n=5) vs HLUI(n=5)*, t-test.

Szczepanski et al., (2024) in preparation

HLUI-mediated muscle disuse effects in mice *TA* are fibre-type dependant.

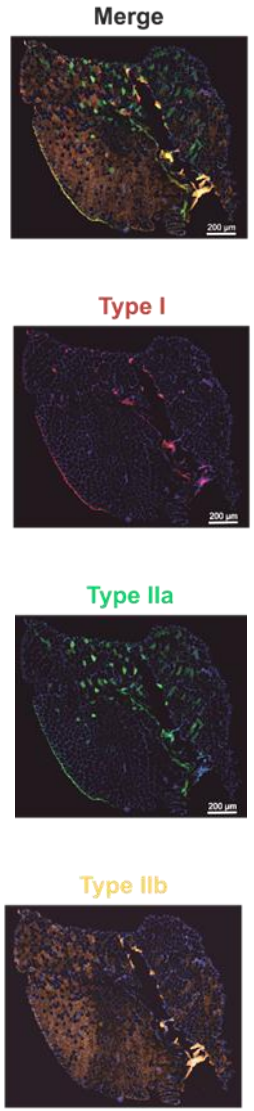

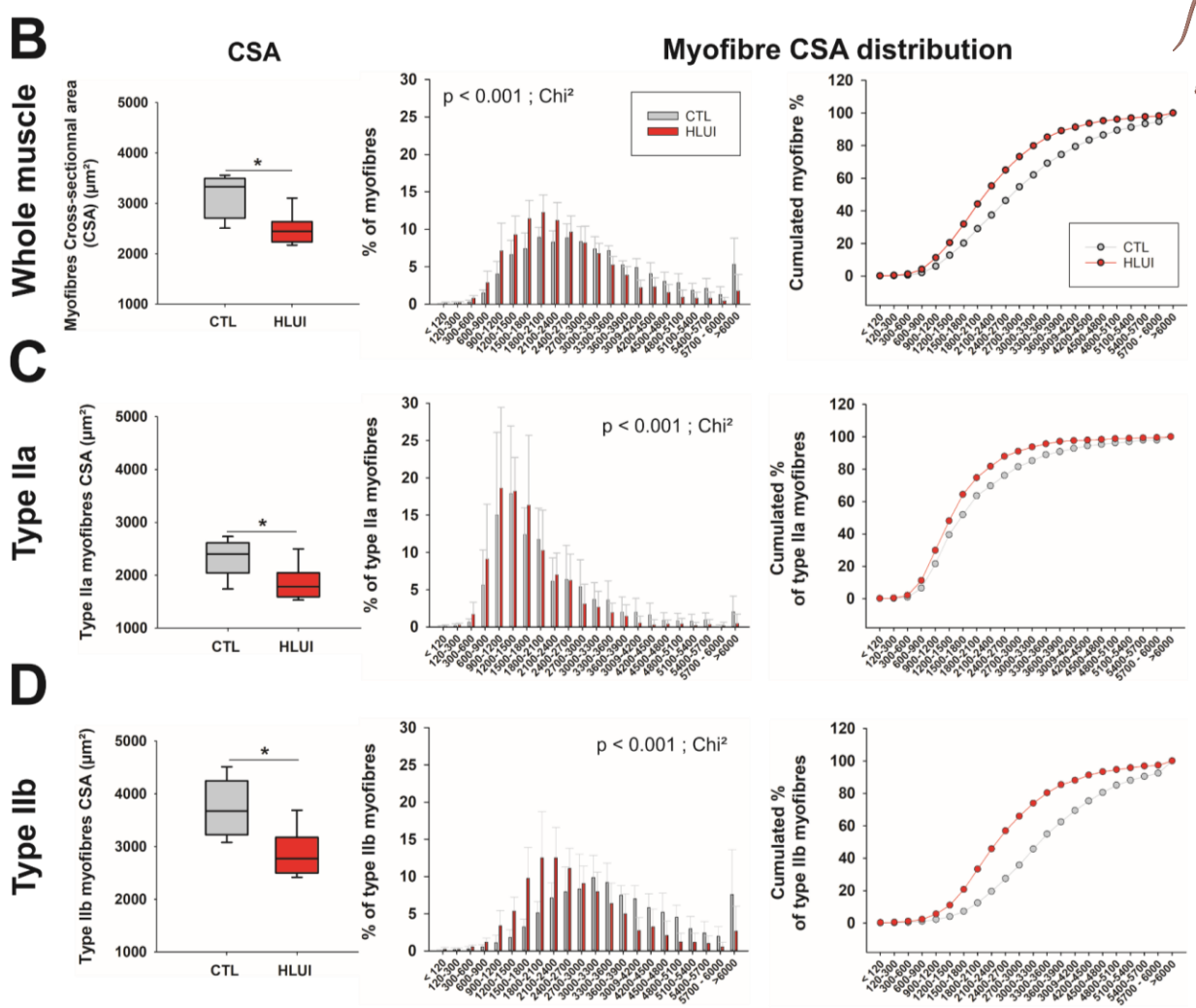

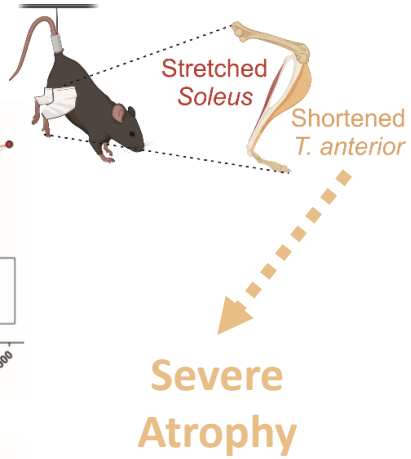

(Left) Data represented as boxplot; *: p<0.05, *CTL(n=5) vs HLUI(n=5)*, t-test.
(Center) Data represented as mean ± SD. *CTL(n=5) vs HLUI(n=5)*, Chi-square.
(Right) Cumulative percentages of myofibres in clusters.

Szczepanski et al., (2024) in preparation

HLUI-mediated muscle disuse effects in mice *TA* are fibre-type dependant.

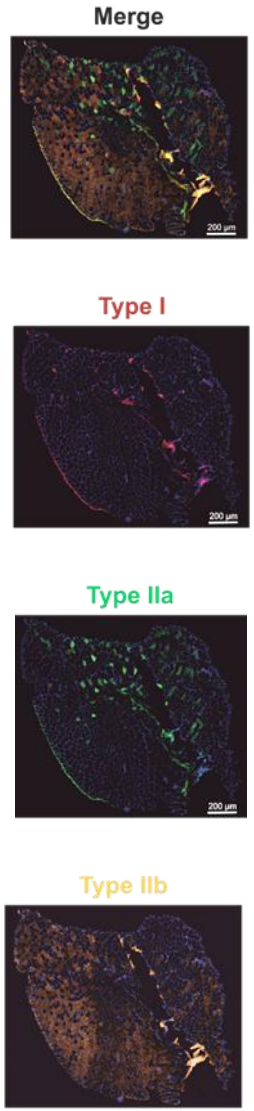

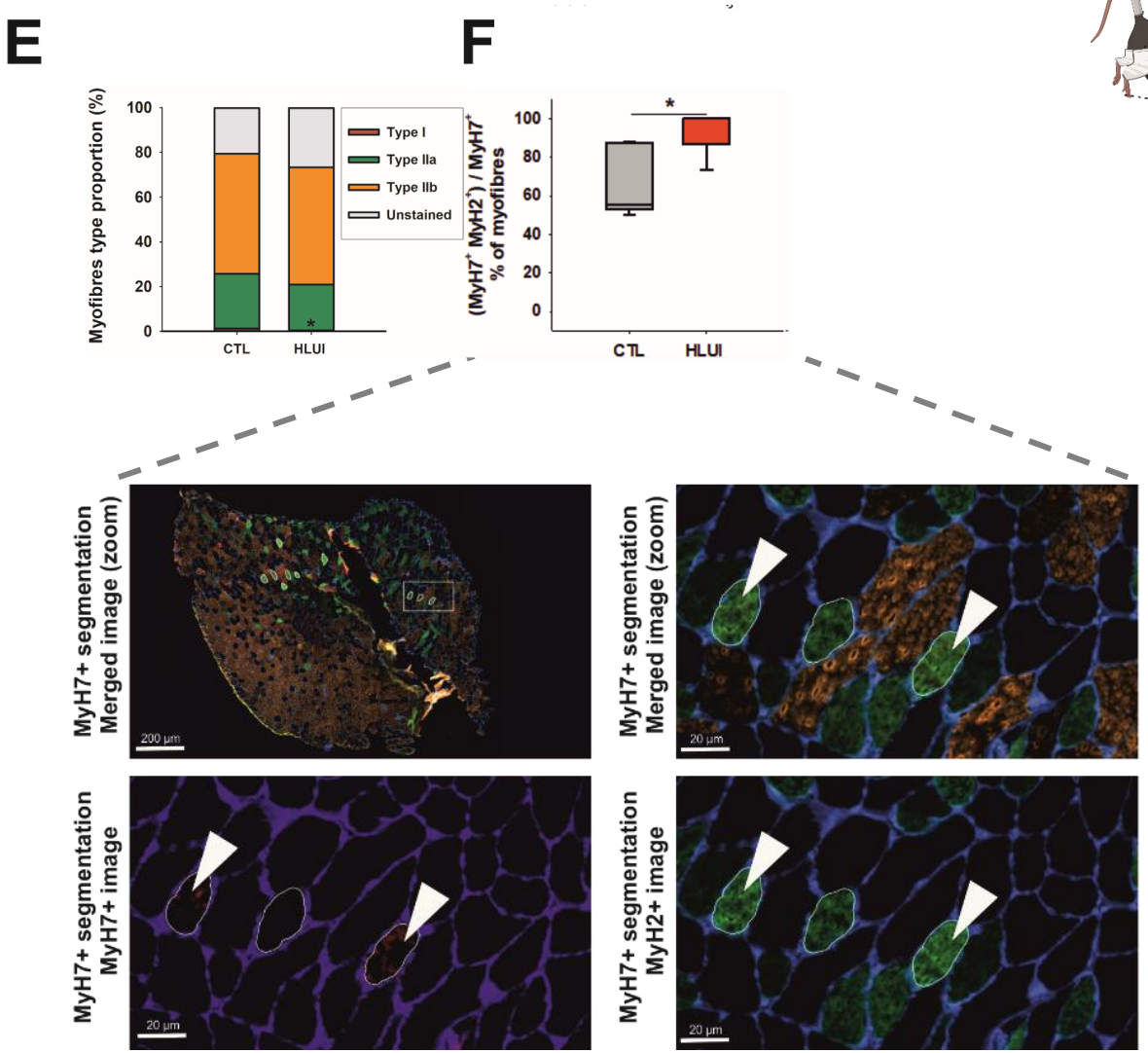

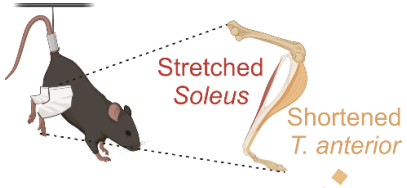

Severe Atrophy + Fiber-type Switch

(E) Data represented as stacked bars; *: p<0.05 *CTL(n=5) vs HLUI(n=5)* in type I, Iia and IIb myofibers, t-test

(F) Data represented as boxplot, *: p<0.05, *CTL(n=5) vs HLUI(n=5)*, t-test.

Szczepanski et al., (2024) in preparation

HLUI-mediated muscle disuse affects ApN plasmatic oligomers distribution.

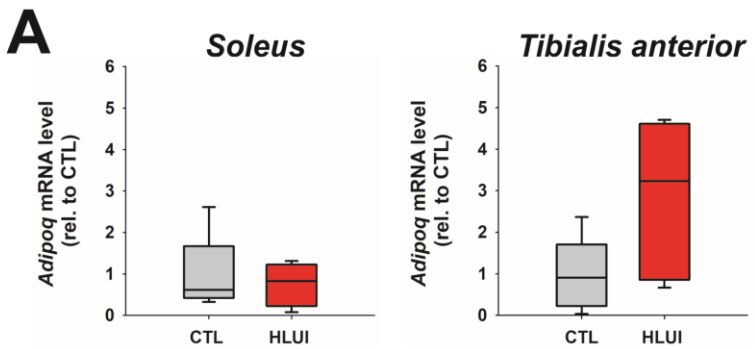

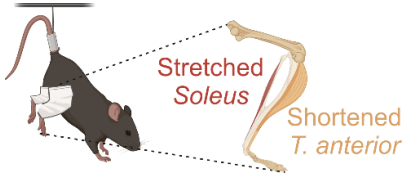

(A) Data represented as boxplot, *CTL(n=6) vs HLUI(n=5)*, t-test: NS.

Szczepanski et al., (2024) in preparation

HLUI-mediated muscle disuse affects ApN plasmatic oligomers distribution.

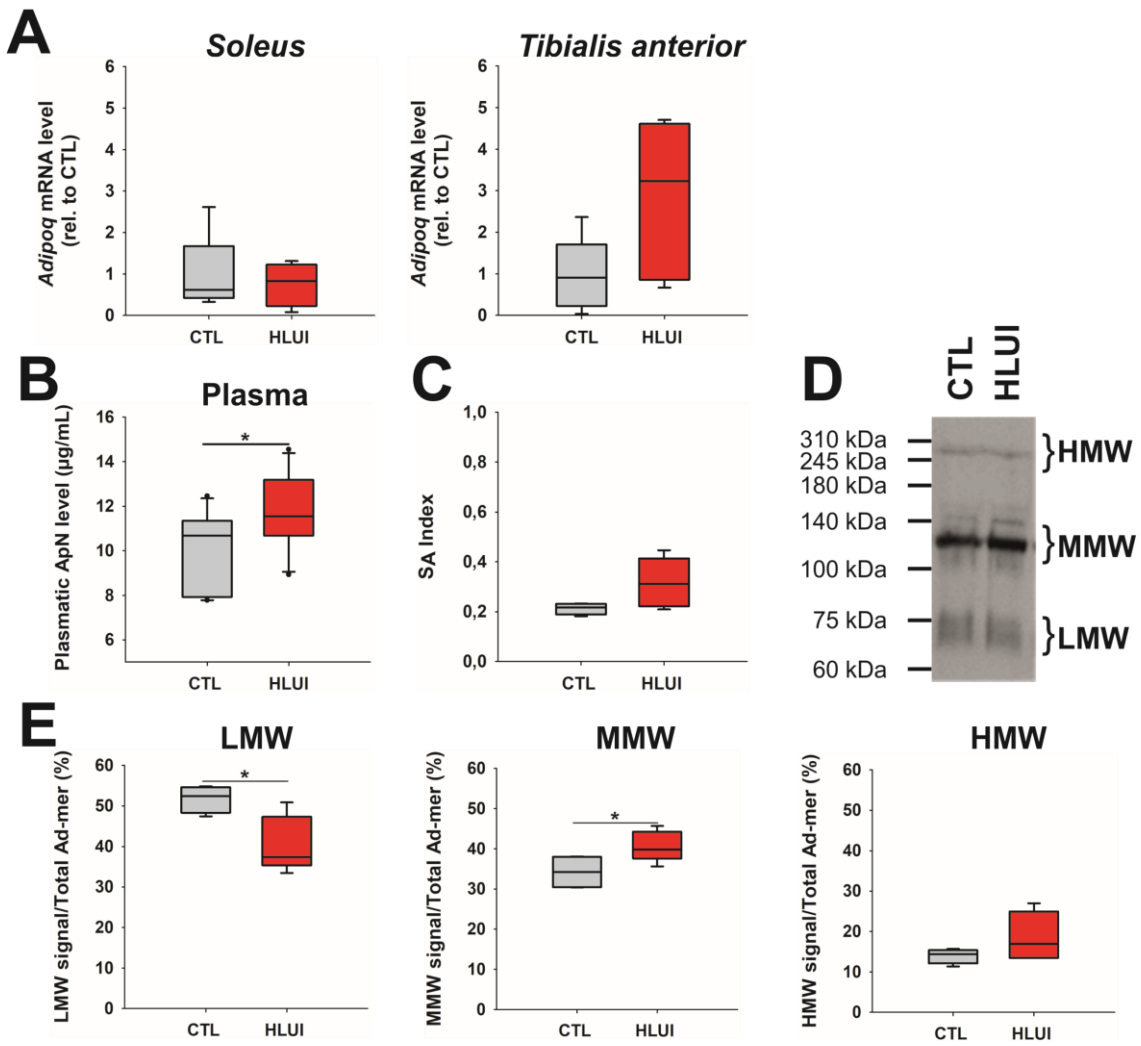

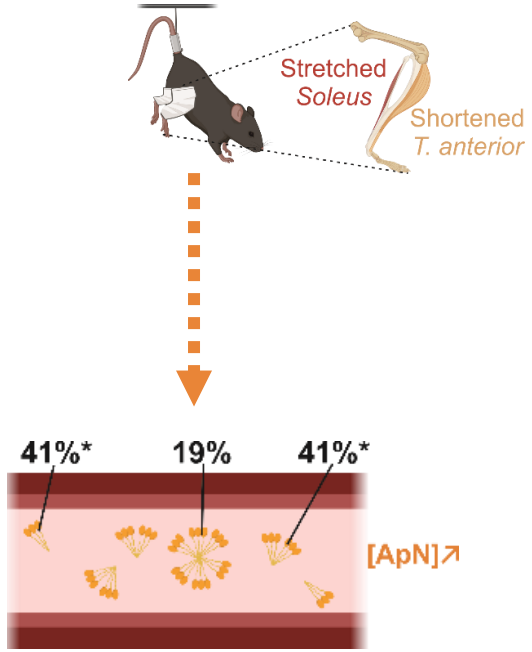

(A) Data represented as boxplot, *CTL(n=6) vs HLUI(n=5)*, t-test: NS.**(B)** Data represented as boxplot; *: p<0.05, *CTL(n=10) vs HLUI(n=11)*, t-test .**(C)** Data represented as boxplot; *CTL(n=4) vs HLUI(n=5)*, t-test: NS. **(E)** Data represented as boxplot; *: p<0.05, *CTL(n=4) vs HLUI(n=5)*, t-test.

Szczepanski et al., (2024) in preparation

HLUI-mediated muscle disuse affects ApN receptors in *Soleus* muscle

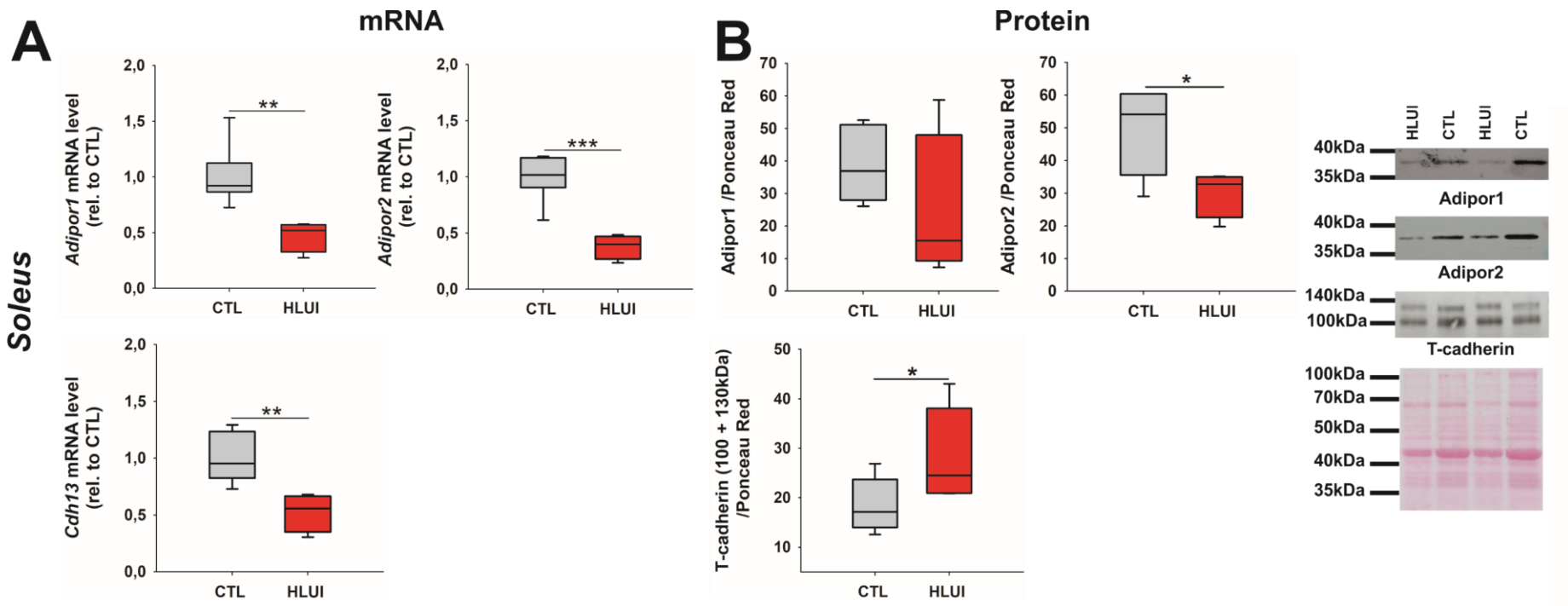

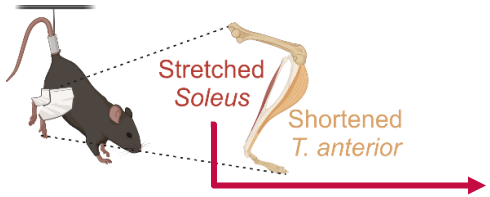

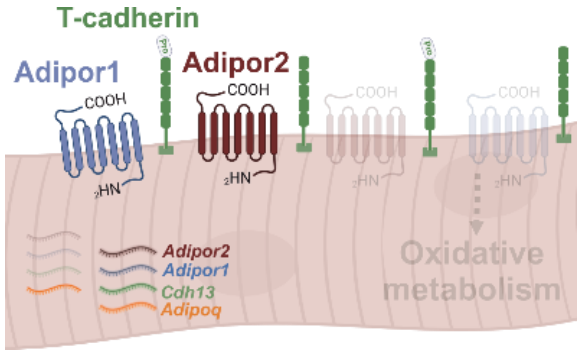

(A) Data represented as boxplot; **: p<0.01, ***: p<0.001, *CTL(n=6) vs HLUI(n=5)*, t-test.
(B) Data represented as boxplot; *: p<0.05, *CTL(n=7) vs HLUI(n=5)*, t-test.

Szczepanski et al., (2024) in preparation

HLUI-mediated muscle disuse has no effect on ApN receptors in *TA* muscle

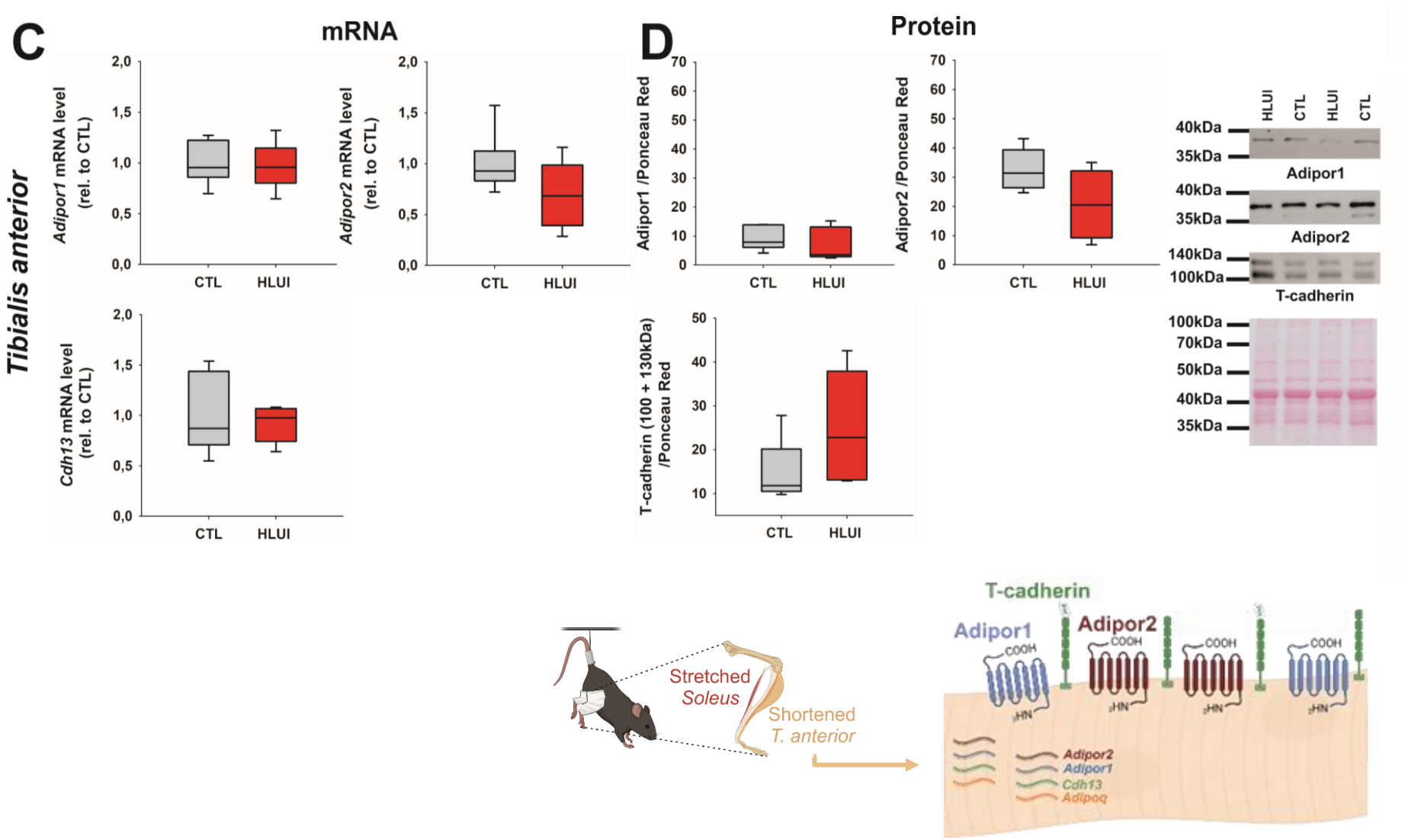

(A) Data represented as boxplot; **: p<0.01, ***: p<0.001, *CTL(n=6) vs HLUI(n=5)*, t-test.

(B) Data represented as boxplot; *: p<0.05, *CTL(n=7) vs HLUI(n=5)*, t-test.

Szczepanski et al., (2024) in preparation

Muscle type determine DMA severity and ApN pathway response to disuse

METHODS

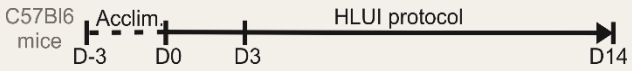

Standard housing

Hindlimb Unloading and Immobilization (HLUI)

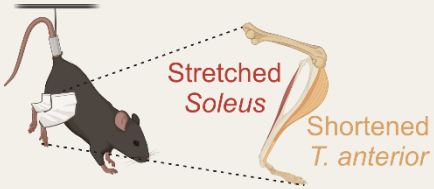

OUTCOME Muscle alterations and ApN pathway in disused muscles

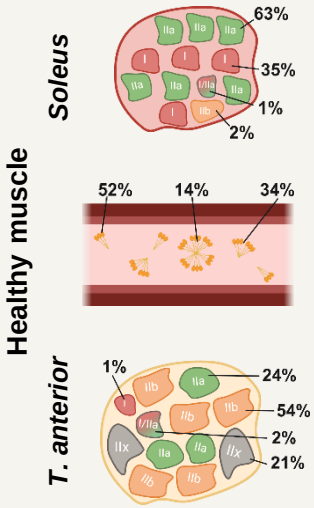

Muscle type determine DMA severity and ApN pathway response to disuse

METHODS

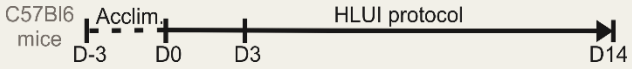

Standard housing

Hindlimb Unloading and Immobilization (HLUI)

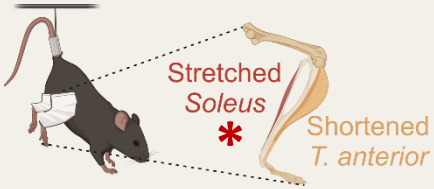

OUTCOME Muscle alterations and ApN pathway in disused muscles

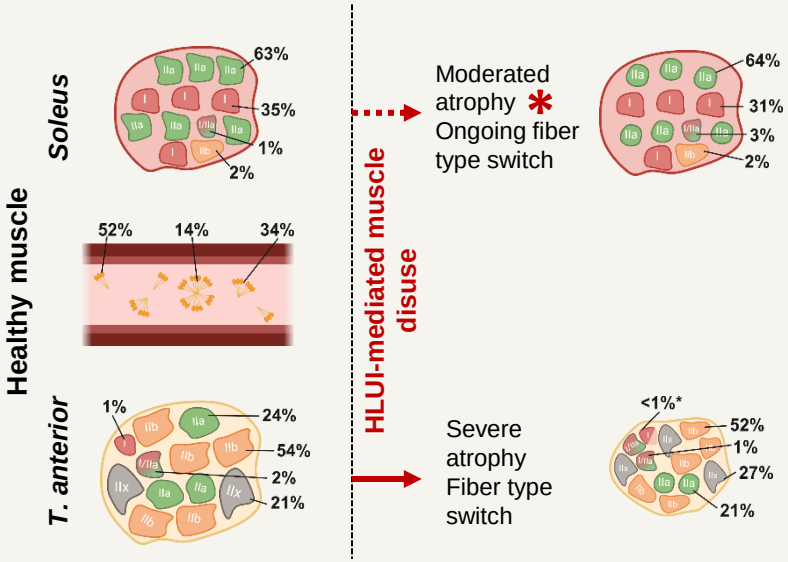

* Persistant isometric contractions

Muscle type determine DMA severity and ApN pathway response to disuse

METHODS

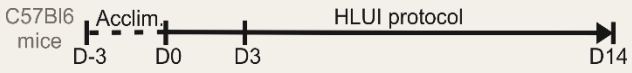

Standard housing

Hindlimb Unloading and Immobilization (HLUI)

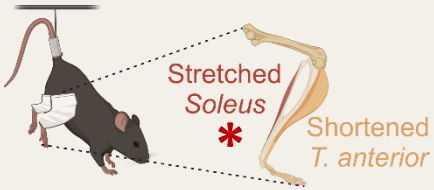

OUTCOME Muscle alterations and ApN pathway in disused muscles

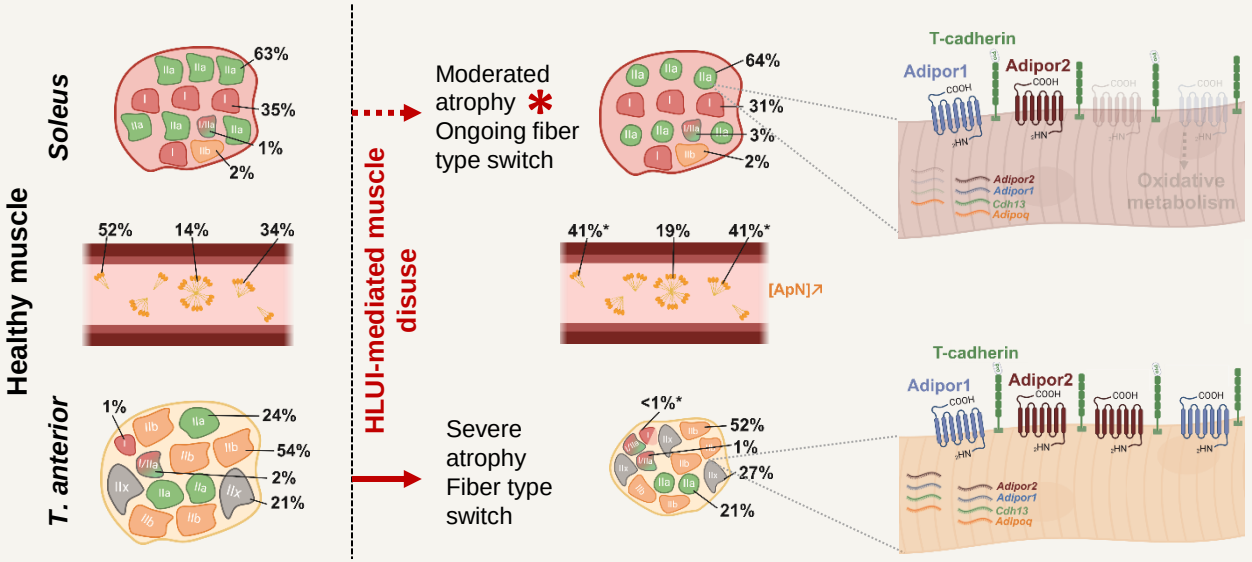

CONCLUSION HLUI is linked to high ApN plasmatic levels but the severity of DMA, the kinetics of myofiber switch and adiporeceptor regulation depend on muscle type and positioning.

*** Persistant isometric contractions**

HLUI-mediated muscle disuse effects mice *Soleus* without ApN ?

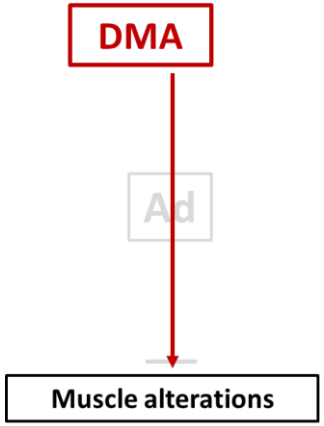

HLUI-mediated muscle disuse affect mice *Soleus* in KO but not in WT mice

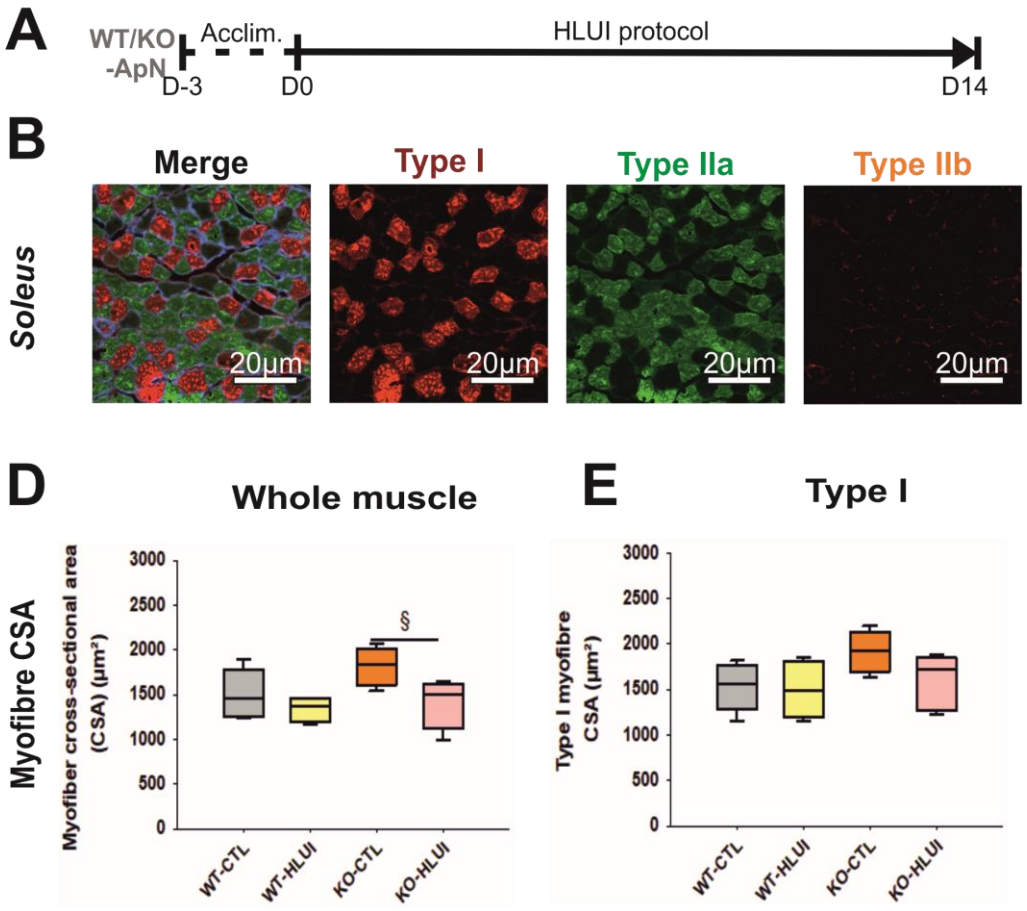

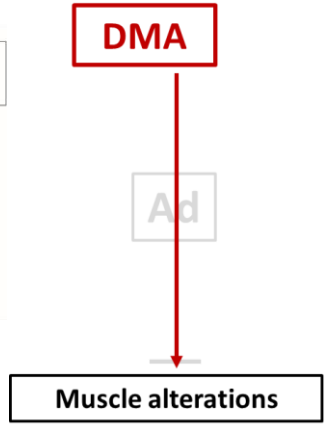

(C) Data represented as stacked bars; **p<0,01 (Genotype effect), ΨΨ p<0,01 (WT-CTLvsKO-CTL), Two-way ANOVA. **(D-F)** Data represented as boxplot. § p<0,05 (KO-CTLvsKO-HLUI), Two-way ANOVA, all pairwise comparison, Holm-Sidak method.

ApN contribution to muscle reconditioning ?

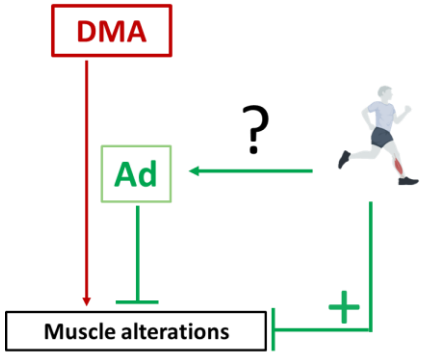

Soleus muscle reconditioning following disuse in KO and WT mice

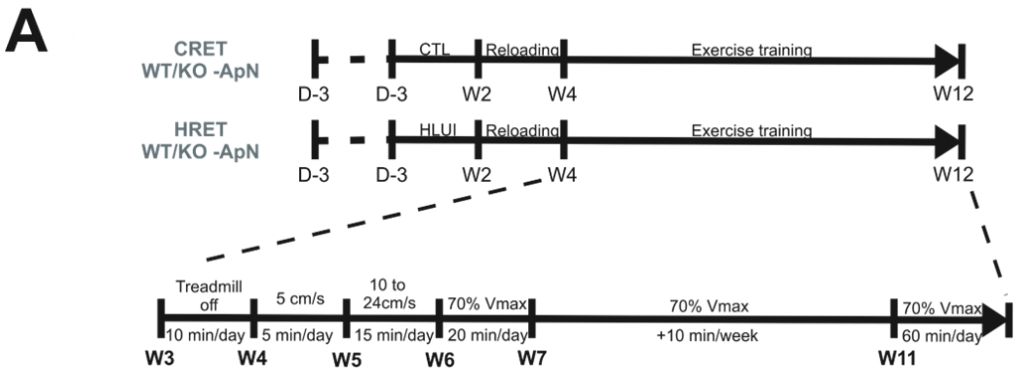

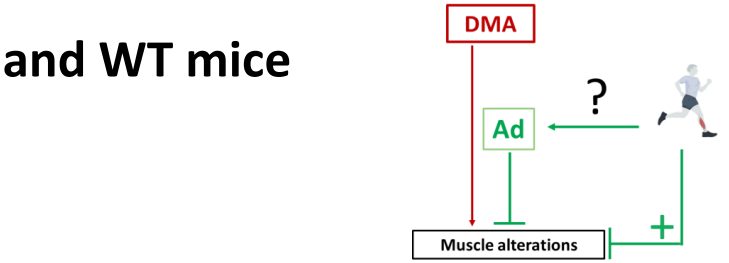

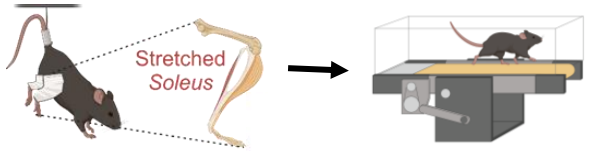

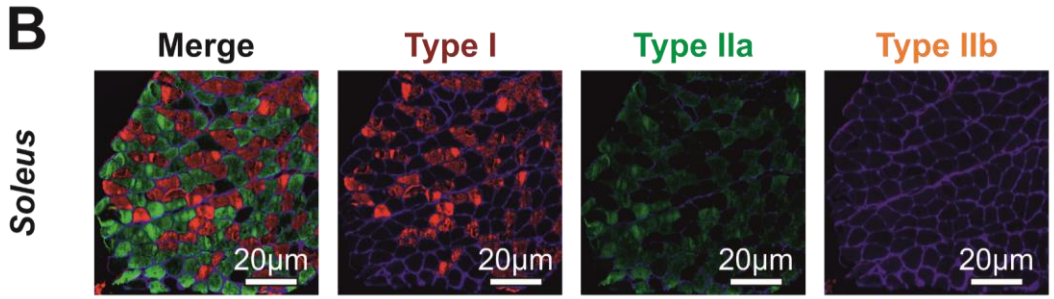

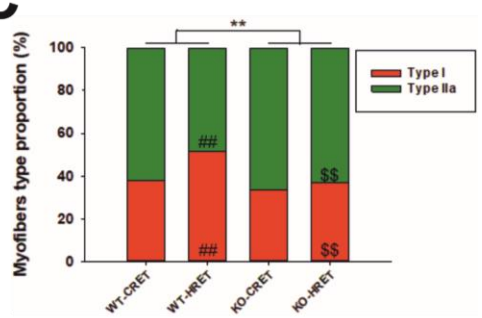

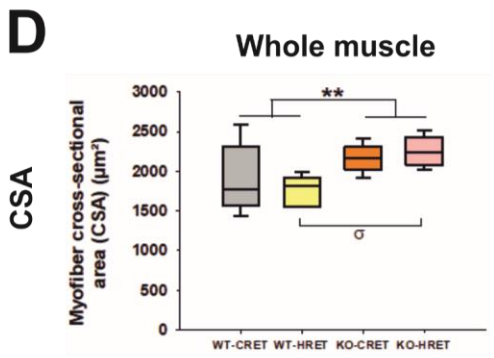

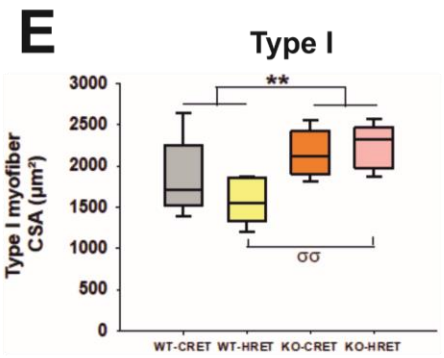

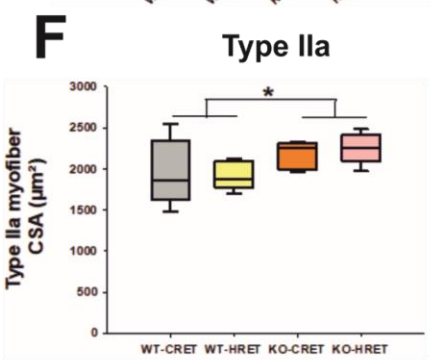

(C) Data represented as stacked bars; **p<0,01 (Genotype effect), $$ p<0,01 (WT-HRETvs KO-HRET), ## p<0,01 (WT-CRETvsWT-HRET), Two Way ANOVA, All pairwwise multiple comparison, Holm Sidak-method. **(D-F)** Data represented as boxplot. *p<0,05; **p<0,01 (Genotype effect); σ p<0,05; σσp<0,01 (WT-HRET vs KO-HRET), Two-way ANOVA, all pairwise comparison, Holm-Sidak method.

HLUI-mediated preconditioning in WT but not in KO mice ?

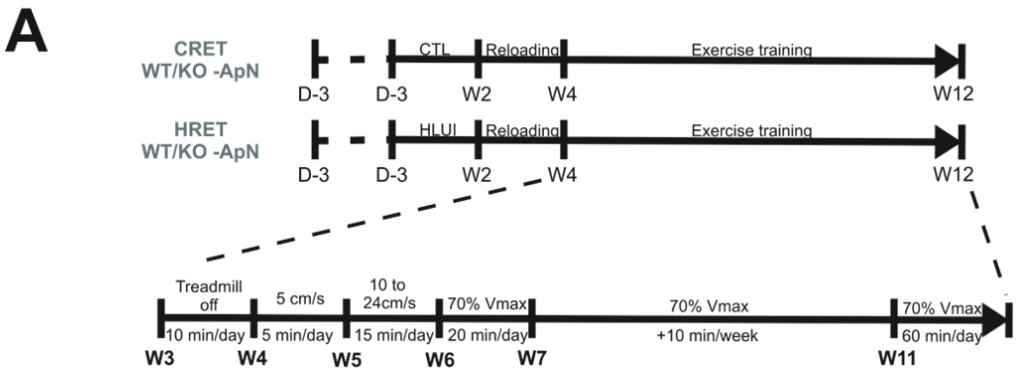

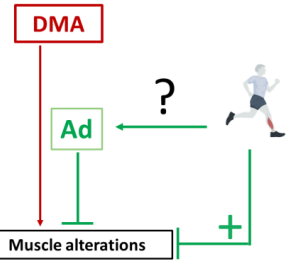

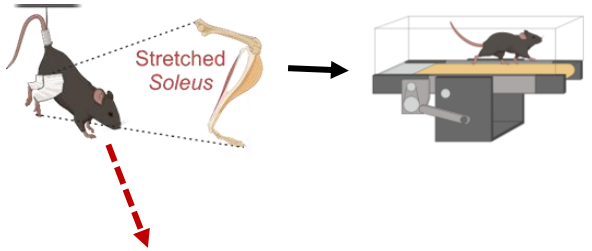

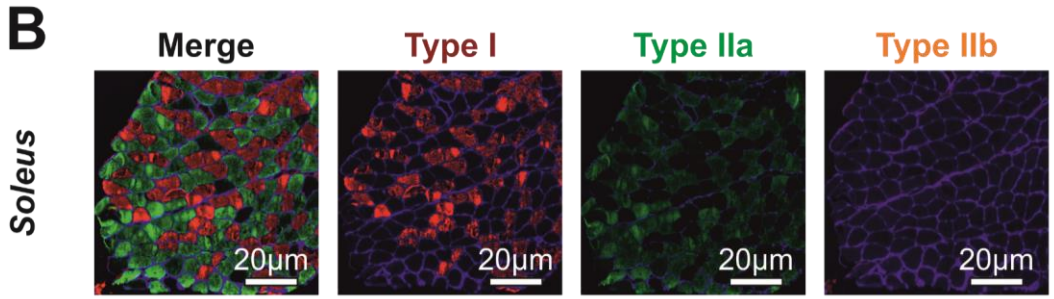

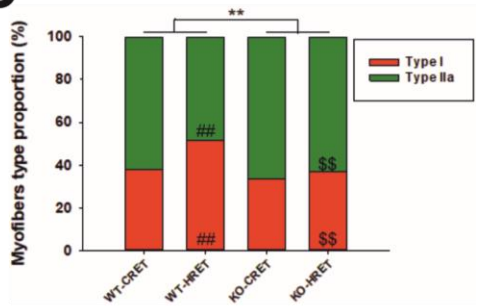

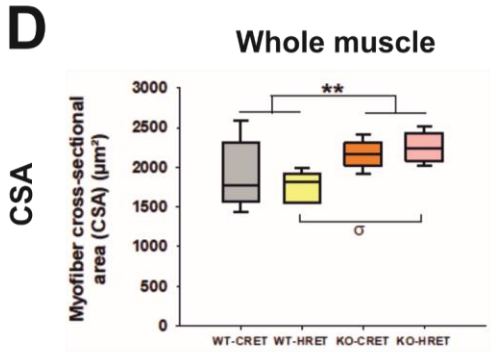

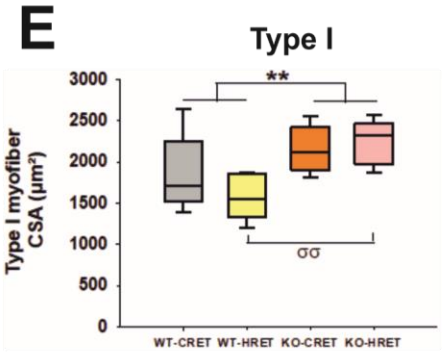

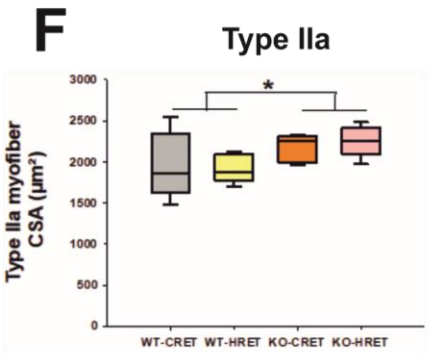

(C) Data represented as stacked bars; **p<0,01 (Genotype effect), $$ p<0,01 (WT-HRETvs KO-HRET), ## p<0,01 (WT-CRETvsWT-HRET), Two Way ANOVA, All pairwise multiple comparison, Holm Sidak-method. **(D-F)** Data represented as boxplot. *p<0,05; **p<0,01 (Genotype effect); σ p<0,05; σσp<0,01 (WT-HRET vs KO-HRET), Two-way ANOVA, all pairwise comparison, Holm-Sidak method.

Thank you for your attention

Acknowledgements to:

- **Prof A. Tassin,**
- **Prof A-E. Declèves,**
- **Prof A. Legrand,**
- **Vincianne Jenart,**
- **Bernard Blairon,**
- **All PhRR and LBMM laboratories members.**

All schematics were created with : bio RENDER

	Soleus			TA		
	Myofibers proportion (%)		*P* Value	Myofibers proportion (%)		*P* Value
	CTL	HLUI		CTL	HLUI	
All myofibers	/	/	/	/	/	/
Type I myofibers	35.34 ± 8.24	32.23 ± 4.43	0.48	1.31 ± 0.81	0.39 ± 0.38	0.04*
Type IIa myofibers	63.05 ± 6.21	65.58 ± 4.27	0.46	24.44 ± 5.30	20.52 ± 10.57	0.47
Type IIb myofibers	1.61 ± 2.54	2.19 ± 2.61	0.69	53.61 ± 8.96	52.50 ± 11.75	0.87
Unstained myofibers	/	/	/	20.64 ± 9.03	26.59 ± 8.76	0.29
Hybrid I/IIa myofibers	1.19 ± 0.55	2.83 ± 1.40	0.41	1.84± 0.87	1.30 ± 1.02	0.43

Table 2. Effect of the HLUI-mediated disuse on myofibers-types proportions in the slow twitch *Soleus* and the fast twitch *TA* muscles. Values are means ± SD; CTL (n=5), HLUI (n=5); (Except in the *Soleus* for type IIb where n=3). CSA, Cross-sectional Area; MFD, Minimum Feret's Diameter; Comparisons made HLUI vs CTL by Student's *t* test or Mann-Whitney Rank Sum test according to the normality assay result.

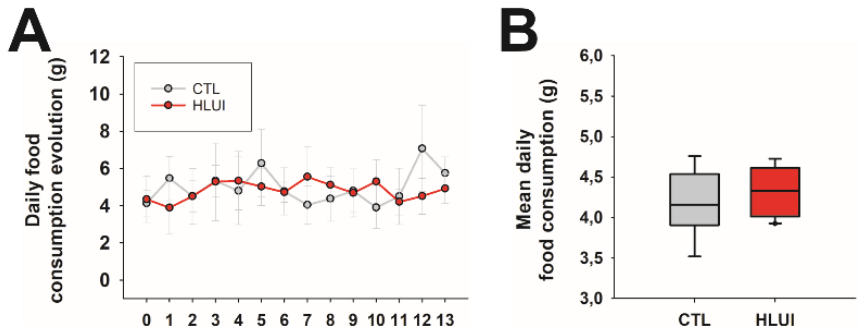

Suppl. Fig 1. Food consumption assessment in CTL and HLUI mice. (A) Food consumption was measured daily. Data plotted as mean ± SD, *CTL(n=10) vs HLUI(n=11)*, ***: p<0.001, Two-way ANOVA repeated measures. **(B)** Mean daily food consumption. Data represented as boxplots; *CTL(n=10) vs HLUI(n=11)*, NS.

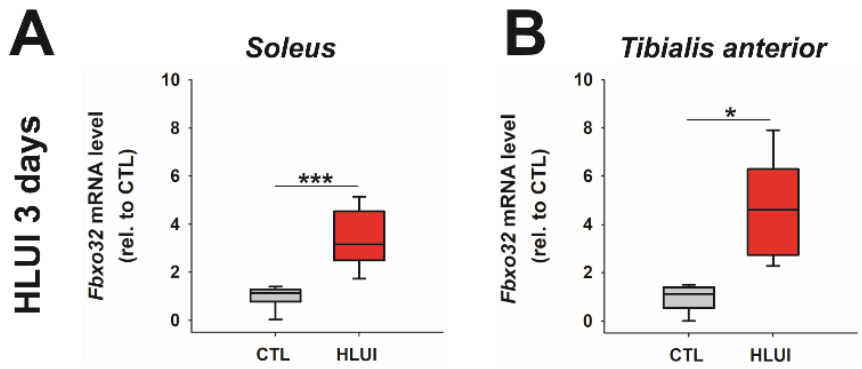

Suppl Fig 2. Early effects of HLUI on *Fbxo 32* expression. *Fbxo 32* mRNA level was assessed in **(A)** the *Soleus* and **(B)** the *Tibialis Anterior* muscles by RTqPCR with ΔΔCt method (housekeeping gene: *Rplp0*; data normalised to CTL). Data represented as boxplot; ***: p<0.001; t-test.

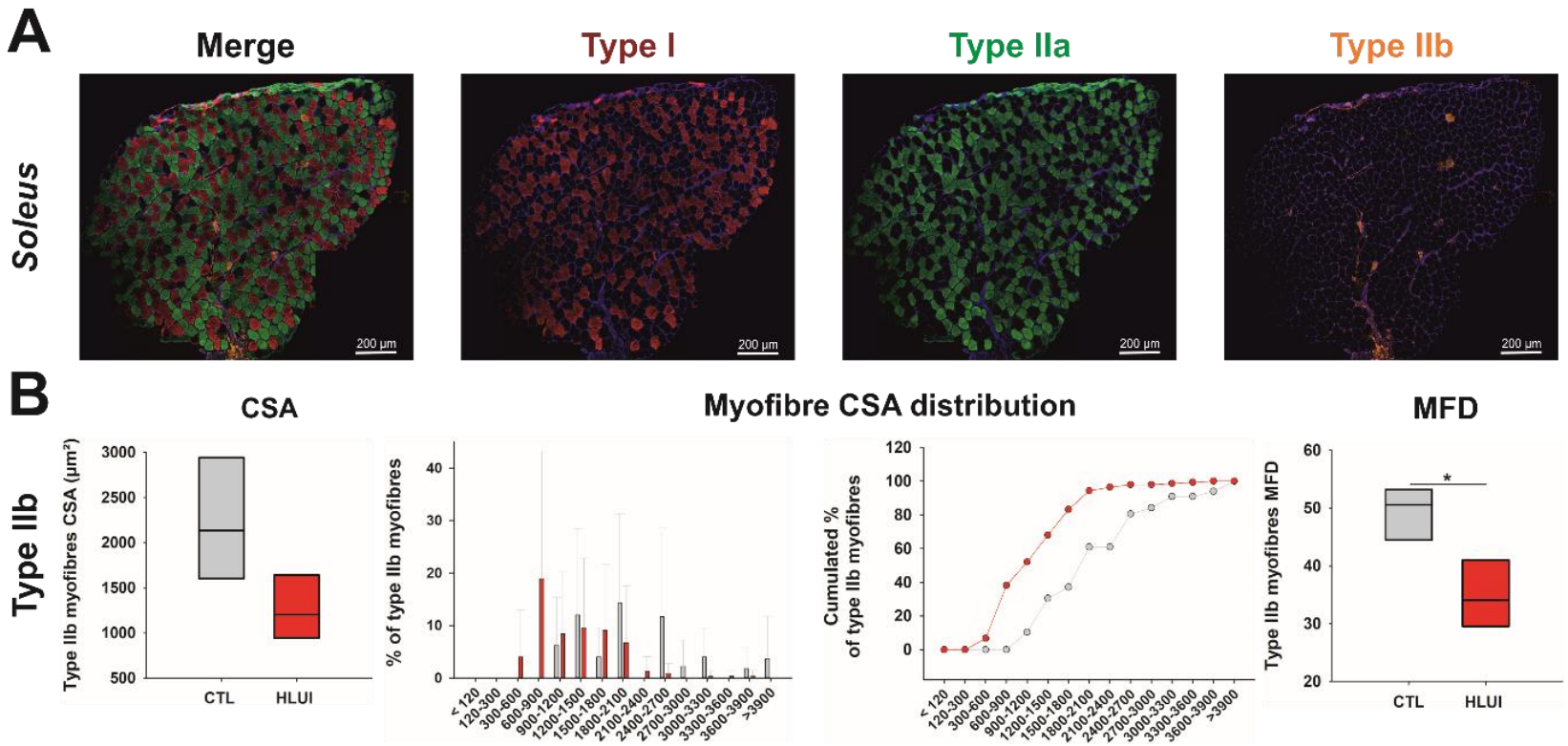

Suppl. Fig 3. Effects of moderate muscle disuse in mice *Soleus* type IIb fibers. Cross-sectional Area (CSA), myofiber CSA distribution and Feret's diameter were measured following type I, IIa and IIb immunofluorescence detection and morphometrical analysis were performed with *Cellpose* and *Image J* softwares. **(A) Representative fields**. **(B)** CSA was mesured in type IIb fibres. Data represented as boxplot, *CTL(n=5) vs HLUI(n=5)*, t-test, NS. **(C)** Type IIb myofibres were classified in clusters according to their area (µm²). Data represented as mean ± SD, *CTL(n=5) vs HLUI(n=5)*, Chi-square was not performed due to the impossibility to have the minimal number of observations required in several clusters. **(D)** Cumulative percentages of type IIb myofibres in clusters. **(E)** Minimim Feret's diametre (MFD) was mesured in type IIb fibres. Data represented as boxplot; *: $p<0.05$, *CTL(n=5) vs HLUI(n=5)*, t-test.

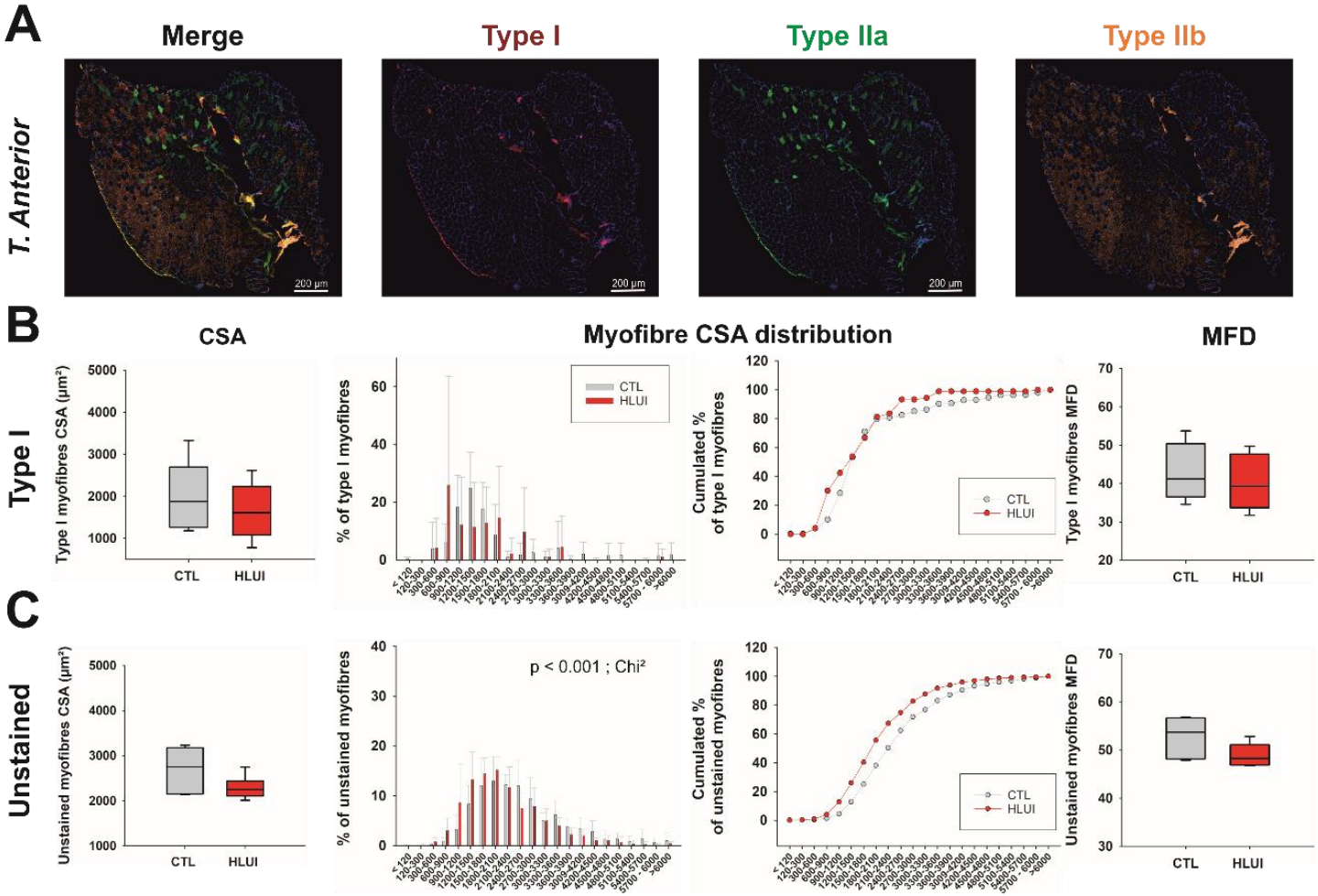

Suppl. Fig 4. Effects of moderate muscle disuse in mice *TA* type I and unstained fibers. Cross-sectional Area (CSA), myofiber CSA distribution and Feret's diameter were measured following type I, IIa and IIb immunofluorescence detection and morphometrical analysis were performed with *Cellpose* and *Image J* softwares. **(A) Representative fields**. **(Left)** CSA was mesured in type I fibers **(B)** and in unstained fibers **(C)**. Data represented as boxplot, *CTL(n=5) vs HLUI(n=5)*, t-test, NS. **(Center)** Myofibers were classified in clusters according to their area (µm²). Type I **(B)** and unstained fibers **(C)**. Data represented as mean ± SD, *CTL(n=5) vs HLUI(n=5)*, Chi-square. Cumulative percentages of myofibres in type I fibers **(B)** and in unstained fibers **(C)**. **(Right)** Minimim Feret's diametre (MFD) was mesured in type I fibers **(B)** and in unstained fibers **(C)**. Data represented as boxplot, *CTL(n=5) vs HLUI(n=5)*, t-test, NS.

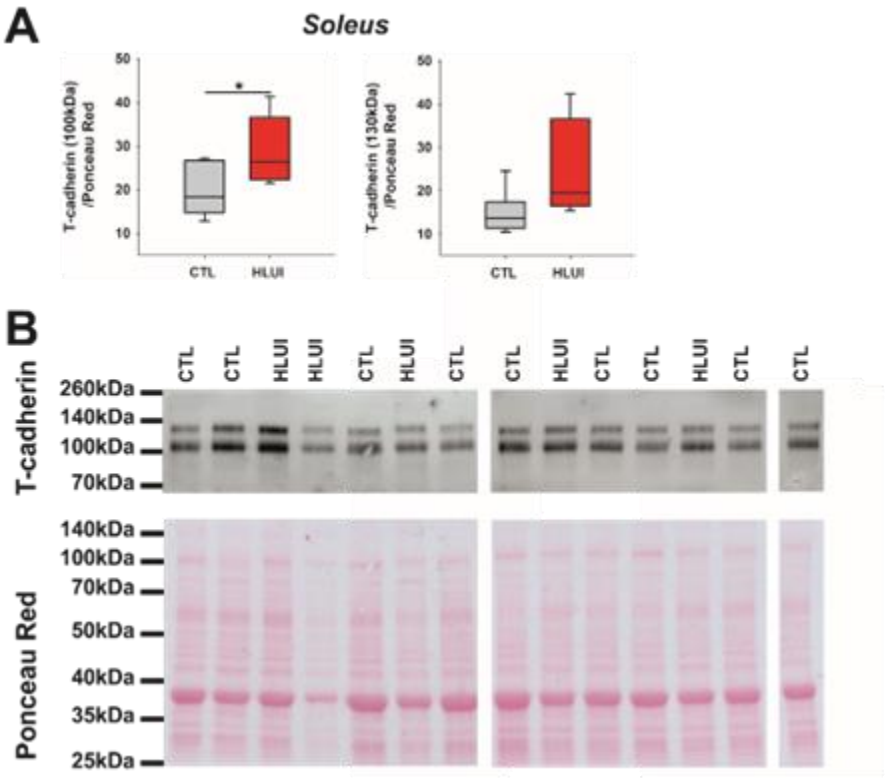

Suppl. Fig 5. (A) Mature (100kDa) and pro-domain bearing (130kDa) T-cadherin protein levels and (B) corresponding westernblot immunodetection and Red Ponceau in the *Soleus* muscle. T-cadherin protein levels were determined using denaturant PAGE-SDS followed by a western blot. Densitometric analyses were performed with *Image J* software. Signal was normalized on Ponceau Red. Data represented as boxplot; *: $p<0.05$, *CTL(n=7) vs HLUI(n=5)*, t-test. **Right,** representative blots.

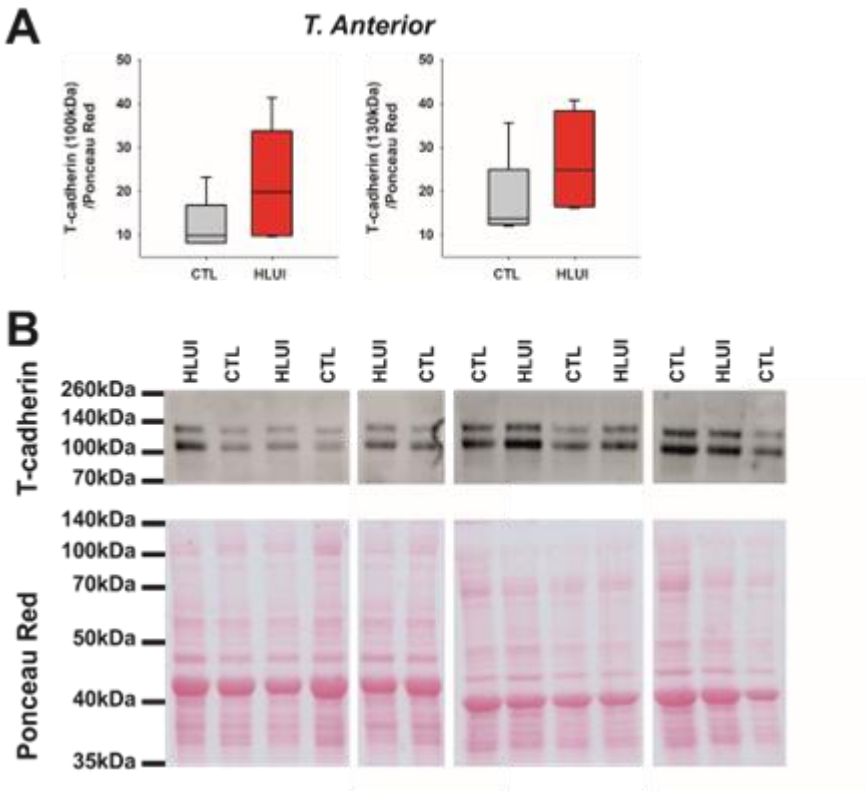

Suppl. Fig 6. (A) Mature (100kDa) and pro-domain bearing (130kDa) T-cadherin protein level and (B) corresponding westernblot immunodetection and Red Ponceau in *Tibialis Anterior muscle*. T-cadherin protein levels were determined using denaturant PAGE-SDS followed by a western blot. Densitometric analyses were performed with *Image J* software. Signal was normalized on Ponceau Red. Data represented as boxplot; *: $p<0.05$, *CTL(n=7) vs HLUI(n=5)*, t-test. **Right,** representative blots.

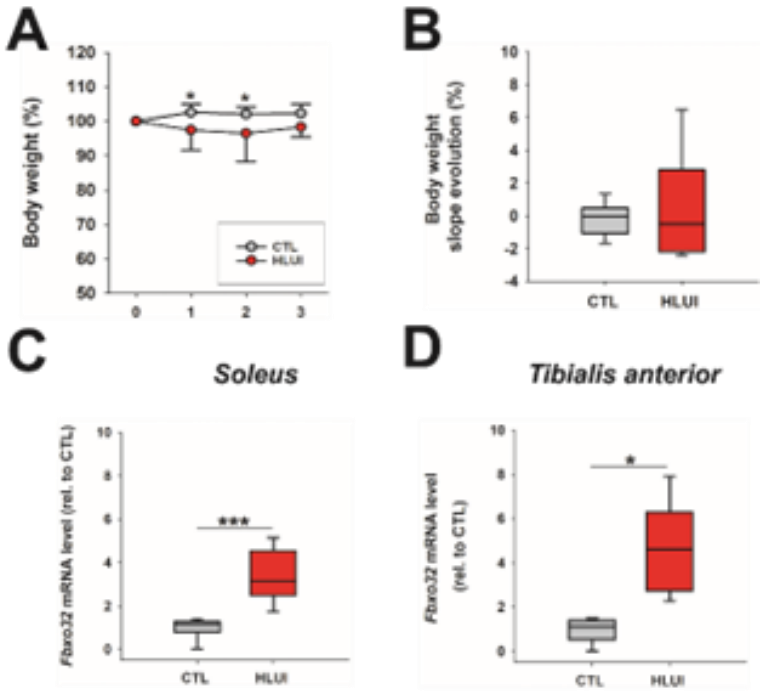

Suppl. Fig 7. Early effects of HLUI on bodyweight evolution and on *Fbxo 32* expression. (A) B.w was measured daily and the first day of protocol (D0) was defined as a 100% baseline. Data represented as mean ± SD, *: p<05, *CTL(n=6) vs HLUI(n=6)*, Two-way ANOVA repeated measures. **(B)** Slope comparison. B.w slope evolution was determined between D1 and D3 of the protocol. Data represented as boxplots; *CTL(n=6) vs HLUI(n=6)*, NS. **(C-D)** *Fbxo 32* mRNA level was assessed in **(C)** the *Soleus* and **(D)** the *Tibialis Anterior* muscles by RTqPCR with ΔΔCt method (housekeeping gene: *Rplp0*; data normalised to CTL). Data represented as boxplot; ***: p<0.001, *CTL(n=6) vs HLUI(n=6)*, t-test.